Planar Photonic Crystal Vertical-Cavity Surface-Emitting Lasers

Meng Peun Tan, *Student Member, IEEE*, Ansas M. Kasten, Joshua D. Sulkin, and Kent D. Choquette, *Fellow, IEEE*

***Abstract*—Planar index-guided proton-implanted photonic crystal vertical-cavity surface-emitting lasers are fabricated and characterized. Index guiding from the photonic crystal improves the performance of the lasers by creating a stable light output versus current response, reducing the threshold current, and enhancing the differential quantum efficiency. Examination of the etch depth dependence of laser efficiency reveals various mechanisms that affect the laser performance and modal properties such as optical loss, Joule heating, and spectral gain-resonance alignment. Photonic crystal designs can be chosen which result in lasing operation only in the fundamental transverse mode from threshold to maximum power, even for the condition of blue-shifted gain spectrum relative to the cavity resonance. Suitable photonic crystal designs are shown to be manufacturable due to the planar device topology, the use of optical lithography in all processing steps, and compatibility with virtually any vertical-cavity surface-emitting laser epitaxial designs.**

***Index Terms*—Index guiding, photonic crystal, single transverse mode, vertical-cavity surface-emitting lasers (VCSELs).**

I. Introduction

VERTICAL-cavity surface-emitting lasers (VCSELs) have emerged as an important light source for short-haul optical data communication, position sensing, biochemical sensing, and imaging applications owing to several advantages such as low-cost fabrication, on-wafer testing, circular beam output, and low operating power. Lasing in multiple transverse modes is a drawback for many applications, although such an emission characteristic is natural due to the relatively large lasing aperture cross section of a VCSEL. Nevertheless, VCSELs operating in the fundamental mode are desired, as high beam quality (i.e., low divergence Gaussian beam) and high spectral purity (single longitudinal and transverse mode) in addition to low power consumption are advantageous in many of the applications mentioned previously.

Lateral selective oxidation and proton implantation have been employed for transverse current confinement in commercially manufactured VCSELs [1]. These two types of confinement are also accompanied by optical waveguiding. Oxide-confined monolithic VCSELs [2] have a stable (with respect to injection current) and relatively large index contrast between the surrounding oxide and the central semiconductor waveguiding region. On the other hand, index guiding in proton-implanted VCSELs [3] relies on the effect of thermal lensing [4], where the refractive index of the core region changes in proportion to the current-induced temperature variation from Joule heating. Due to the lack of stable index guiding in implanted VCSELs, they tend to possess higher threshold current, unstable beam profile, and a turn-on delay in response to pulsed excitation [5] when compared to oxide-confined VCSELs. In terms of modal properties, oxide-confined VCSELs typically operate multimode due to the high index contrast, whereas for proton-implanted VCSELs, the fundamental mode dominates at low injection level but higher order modes emerge as the bias current is increased due to stronger thermal lensing and spatial hole burning [1].

Numerous efforts have been reported to obtain stable fundamental mode lasing in VCSELs. The approaches to promote single-mode lasing include 1) creating a waveguide that only supports the fundamental mode (e.g., having a small oxide or implant aperture); 2) preferentially pumping the fundamental mode by creating a gain area smaller than the optical aperture [6], [7]; and 3) introducing greater losses such as diffraction loss [8], scattering loss [9], free carrier absorption [10], [11], antiguiding [12], [13], and mirror loss [10], [11], [14]–[17] to the higher order modes. Nevertheless, not all of these methods produce high side-mode suppression ratio (SMSR) or maintain single-mode lasing throughout the whole operating current range, and the majority require additional fabrication steps or specialized epitaxial structure with feature sizes dependent on the lasing wavelength, all of which complicates manufacturability. Using a small diameter oxide or implant aperture is known to increase the series resistance leading to undesirable device heating, as well as excessive current density which can degrade VCSEL reliability [18].

In this study, the photonic crystal structure is employed to achieve single-mode emission in VCSELs [19]–[27]. A periodic pattern of air holes etched into the output distributed Bragg reflector (DBR) mirror with one central air hole removed to form the lasing defect is a method for creating fundamental

Manuscript received November 1, 2012; revised December 19, 2012; accepted January 8, 2013. This work was supported by the National Science Foundation under Award DMI 0749028.

M. P. Tan and K. D. Choquette are with the Department of Electrical and Computer Engineering, University of Illinois at Urbana-Champaign, Urbana, IL 61801 USA (e-mail: mengtan@illinois.edu; choquett@illinois.edu).

A. M. Kasten was with the Department of Electrical and Computer Engineering, University of Illinois, Urbana, IL 61801 USA. He is now with General Electric Global Research Center, Niskayuna, NY 12309 USA (e-mail: kasten@ge.com).

J. D. Sulkin was with the Department of Electrical and Computer Engineering, University of Illinois at Urbana-Champaign, Urbana, IL 61801 USA. He is now with Space Exploration Technologies Corporation, Hawthorne, CA 90250 USA (e-mail: josh.sulkin@gmail.com).

Color versions of one or more of the figures in this paper are available online at http://ieeexplore.ieee.org.

Digital Object Identifier 10.1109/JSTQE.2013.2241398

mode VCSEL operation that uses the concepts of single-mode waveguide and loss selectivity [22], [27]. The etched photonic crystal provides optical confinement with an engineered transverse step-index profile which is stable with respect to the injection current. The electrical confinement is created using ion implantation; by separating the electrical and the optical apertures, a larger current aperture can be made, resulting in lower series resistance and reduced current density for single-mode VCSELs [24]. There is no requirement imposed on the epitaxial design to fabricate photonic crystal VCSELs, and the photonic crystal design parameters can be independent of the lasing wavelength for a wide range of wavelength and etch depth [25]. Moreover, we will show that single-mode operation can be obtained for the condition of a spectrally blue-shifted gain peak relative to the cavity resonance, a strategy that is commonly employed for high-temperature operation [28] but often results in higher order lasing modes [29]. Using proton implantation for current confinement, it was previously shown that the threshold current and the differential quantum efficiency can be improved in photonic crystal VCSELs, because the gain guiding of proton-implanted VCSELs is overcome by introducing index guiding from the etched photonic crystal [24]. Proton-implanted VCSELs are known to be extremely reliable with superior lifetimes [30], and adding photonic crystal to the VCSELs should not compromise the reliability based on the reports of Kasten *et al.* [26].

The majority of prior photonic crystal VCSELs used oxide-confined apertures and electron beam lithography to define the hole patterns [19]–[24]. The photonic crystal VCSELs reported herein utilize both current and optical apertures defined by optical lithography. Consequently, the photonic crystal VCSELs exhibit index-guiding performance, yet are planar, manufacturable, and should yield high reliability. In this paper, the design and fabrication of photonic crystal VCSELs are reported in Section II. The performance of the lasers fabricated from commercial VCSEL epitaxial materials is discussed in Section III, where the influence of index guiding is investigated by varying the etch depth of the photonic crystal. We report relatively high single-mode output power from photonic crystal VCSELs with manufacturable designs, and conclude in Section IV.

II. Device Designs and Fabrication

Proton-implanted photonic crystal VCSELs fabricated from many different wafers with various epitaxial structures have been studied; here, we present the characteristics of two samples. Both VCSEL wafers contain a p-type top DBR mirror, a single-wavelength long optical cavity containing GaAs quantum wells, and an n-type bottom DBR mirror grown on an n-type GaAs substrate. Sample A has 21 linearly graded $Al_{0.12}Ga_{0.88}As$/AlAs top DBR periods, whereas Sample B contains 20 top DBR periods of linearly graded $Al_{0.12}Ga_{0.88}As$-$Al_{0.9}Ga_{0.1}As$ layers; hence, the output mirror of Sample A has higher refractive index contrast and greater mirror reflectivity. Sample A also has a gain peak that is significantly spectrally blue-shifted with respect to the cavity resonance, which tends to promote multimode and higher order mode lasing because the higher order modes have greater spectral overlap with the gain than the fundamental mode [29].

The hexagonal-lattice photonic crystal pattern has two lithographically determined parameters: hole diameter b and hole pitch a. Nine photonic crystal designs are considered: $b/a = 0.6$, $a = 3$, 3.5, 4, 4.5, and 5 μm; and $b/a = 0.7$, $a = 3$, 3.5, 4, and 4.5 μm. These designs yield single-mode lasing for a wide range of etch depth in oxide-confined photonic crystal VCSELs [25], and correspond to designs that are conducive to optical lithography and inductively coupled plasma reactive-ion etching (ICP-RIE). Furthermore, these photonic crystal designs produce index-confined cavity diameters in the range of 4–7 μm, which are relatively broad area. The lithographically defined current aperture is designed to be $2b$ larger than the optical aperture. For Sample A, the photonic crystal etch depth is through the top DBR stopping at the optical cavity. For Sample B, several etch depths are produced by varying the photonic crystal etch time to study the etch depth dependence of differential quantum efficiency and threshold current of the photonic crystal VCSELs. For both wafer samples for all device designs, gain-guided VCSELs that only have the proton-implanted gain aperture are also fabricated.

Fabrication begins with deposition of broad-area AuGe–Ni–Au n-type metal contact on the substrate and Ti–Au p-type top ring contacts on the top DBR. Next, the current apertures are defined by photolithography by patterning of thick photoresist masks to block high-energy (340 keV) proton implantation. The VCSELs are isolated electrically in a second implantation step using another resist mask for a multiple stack of ion implantations with different ion species, energy, and dose [1]. Optical lithography is employed to create the photonic crystal patterns in a deposited SiO_2 layer, which is subsequently used as the etch mask for ICP-RIE of the air holes. A cross-sectional sketch and top-view scanning electron microscope image of a proton-implanted photonic crystal VCSEL in Fig. 1 shows the planar VCSEL profile. Finally, wire bonding metal pads are added on top of a dielectric layer (not shown in Fig. 1). The fabrication processes are identical to those used in commercial VCSEL manufacture and all of the dimensions of the optical lithography are insensitive to the laser wavelength of operation.

III. Experimental Results

Gain-guided implanted VCSELs exhibit disadvantages compared to index-guided VCSELs due to their lack of stable index confinement. These include variable beam steering during current injection, often also accompanied by instability in the light output versus current (L–I) curve (e.g., dramatic fluctuations of differential quantum efficiency) [5], as well as diffraction loss at threshold leading to higher threshold under pulsed excitation as compared to continuous wave operation [4]. By contrast, etching the air hole photonic crystal pattern into the top DBR provides stable and symmetric index guiding, thereby stabilizing the differential quantum efficiency and reducing the threshold current. Fig 2(a) shows the L–I and Fig. 2(b) exhibits the lasing spectra at the maximum output power for a photonic crystal VCSEL ($b/a = 0.6$ and $a = 3.5$) and an implanted VCSEL with

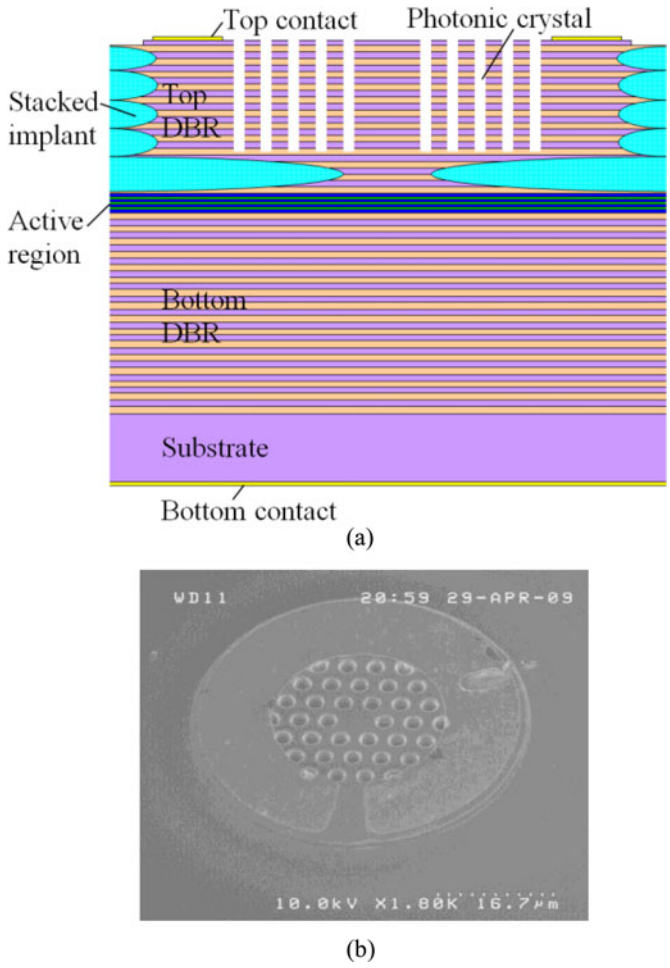

Fig. 1. (a) Cross-sectional sketch and (b) top-view scanning electron microscope image of a planar implant-confined photonic crystal VCSEL.

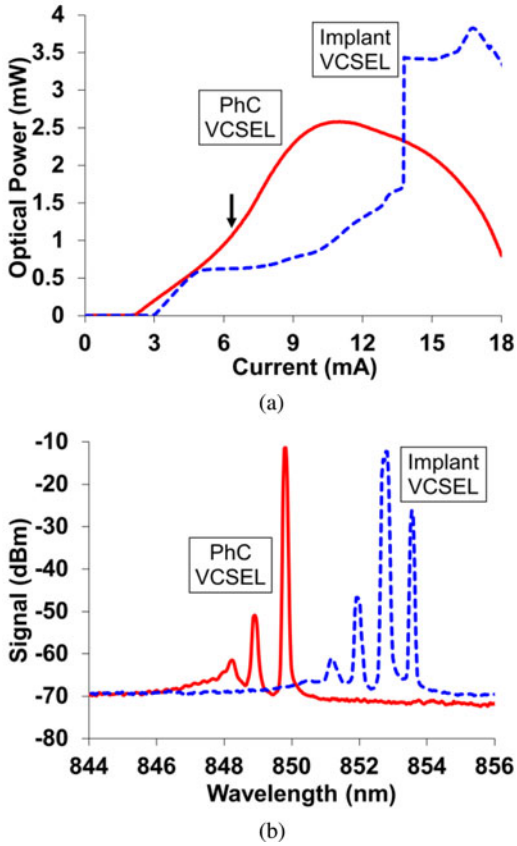

Fig. 2. (a) Light output power versus current and (b) lasing spectra of a proton-implanted VCSEL fabricated in Sample A before (dashed curves) and after (solid curves) etching the photonic crystal pattern ($b/a = 0.6$ and $a = 3.5$) showing single-mode operation; the spectra in (b) are measured at the maximum output power of the VCSELs.

an identical gain aperture (implant diameter ≈ 9 μm) fabricated from Sample A. Comparing the output curves in Fig. 2(a), the L–I discontinuity of the proton-implanted VCSEL at 14 mA is eliminated after the air holes are etched, but the current for maximum power is reduced due to Joule heating effects that arise from increased series resistance. The threshold current is decreased from 3 to 2.1 mA with the addition of the photonic crystal pattern due to its concomitant index confinement. From Fig. 2(b), we see that fundamental mode operation dominates the photonic crystal VCSEL over its entire operation range, whereas the implanted VCSEL at maximum power has multiple transverse modes where a higher order mode is dominant. In this paper, an SMSR $\geq$30 dB between the fundamental and the higher order modes over the entire operating current range (from threshold to maximum of output power) is the criterion for single fundamental mode operation. The slope efficiency and power reduction of the photonic crystal VCSEL compared to the implanted VCSEL is expected due to the discrimination of the higher order modes; note that the implanted VCSEL shows that a higher order mode is the dominant lasing mode, which is suppressed by $>$30 dB after the photonic crystal etching. The photonic crystal VCSEL in Fig. 2(a) has a maximum output power greater than 2.5 mW in the fundamental mode. On this Sample A wafer, we obtain numerous single-mode photonic crystal VCSELs with threshold current less than 2 mA and exhibiting $\geq$2 mW output power.

The photonic crystal VCSEL in Fig. 2 has an optical aperture diameter of $2a-b = 4.9$ μm, whereas the nominal implant aperture diameter is about 9 μm. Consequently, we expect reduced differential quantum efficiency and output power due to the smaller mode size relative to current aperture size [31], [32] which creates a carrier shunt path around the lasing spot. Therefore, larger current aperture enables lower current density and series resistance but also results in reduced efficiency.

It should be noted that this wafer has a significant spectral blue shift of the gain relative to the cavity resonance ($>$20 nm); as a result, higher order modes enjoy greater modal gain, which is evident by the dominance of higher order modes in the spectrum of the implanted VCSELs. Nevertheless, the photonic crystal patterns introduced into these devices as shown in Fig. 2 maintain single fundamental mode operation. For VCSELs fabricated from Sample A, we observe an increase in differential quantum efficiency with increasing current in single-mode photonic crystal VCSELs [see the arrow in Fig. 2(a)]. This is not the same behavior often found in multimode VCSELs in which kinks in the light output curve appear due to the onset of higher order modes, or in proton-implanted VCSELs that lack index guiding

[e.g., the discontinuity of the dashed curve in Fig. 2(a)]. Instead, for single-mode VCSELs, this phenomenon arises from the gain peak shifting into spectral alignment with the lasing mode at higher temperature, causing the differential quantum efficiency to increase with current.

In addition to the photonic crystal parameters, the hole etch depth is the remaining fabrication variable. Fig. 3 shows the variation of the differential quantum efficiency and threshold current as a function of etch depth (normalized to the top DBR thickness) for proton-implanted control and photonic crystal VCSELs ($b/a = 0.7$, $a = 4$ and 4.5 μm) fabricated in Sample B. Note that due to the range of etch depths, not all the VCSELs shown in Fig. 3 operate in the single fundamental mode. The gain-guided (proton-implanted only, 0% etch depth) VCSELs with the same implant aperture show a wide range of differential quantum efficiency and threshold current in Fig. 3, and this variation is randomly distributed across the sample, which indicates that such statistical distribution is not due to a systematic variation of epitaxial layer thickness [33]. It is apparent in Fig. 3 that with deeper photonic crystal air holes, the distributions of differential quantum efficiency and threshold current (standard deviation shown by the dashed lines) are reduced, indicating stronger index guiding introduced by the photonic crystal and diminishing influence of thermal lensing as etch depth increases. Note that in Fig. 3, there are more photonic crystal VCSELs with 100% etch depth than implanted (0% etch depth) VCSELs, and yet the distributions of differential quantum efficiency and threshold current of the photonic crystal VCSELs are considerably narrower.

The photonic crystal structure introduces a step-like transverse index profile which can be modeled as an optical fiber where the core is the unetched semiconductor and the cladding is the photonic crystal region [21], [27]. The index contrast between the core and the cladding Δn can be calculated using the effective index method [34] which accounts for the finite air hole etch depth during the transfer matrix calculation of the cladding index [27]. In Fig. 4, we plot the index contrast as a function of the hole depth (normalized to the top DBR thickness) for photonic crystal VCSELs fabricated from Sample B. The calculated index contrast between the core and the cladding in Fig. 4 monotonically increases with photonic crystal etch depth, but requires hole depths of greater than 60% of the DBR for an appreciable value. This calculation is slightly different from the previous work in which an etch depth dependence parameter γ proportional to the longitudinal standing wave intensity is used to calculate the cladding index [21]. Nevertheless, Fig. 4 closely resembles the results determined using the etch depth dependence parameter (see Fig. 9 of [21]), indicating the equivalence of both methods. In fact, Δn calculated using the effective index method is just the index contrast obtained assuming infinite etch depth multiplied by γ

$$\begin{aligned}\Delta n &= n_{\text{core}} - n_{\text{clad}} = n_{\text{core}} - ((1-\gamma)n_{\text{core}} + \gamma n_{\text{core,holes}}) \\ &= \gamma(n_{\text{core}} - n_{\text{core,holes}}) \\ &= \gamma \Delta n_{\text{eff}} \end{aligned} \quad (1)$$

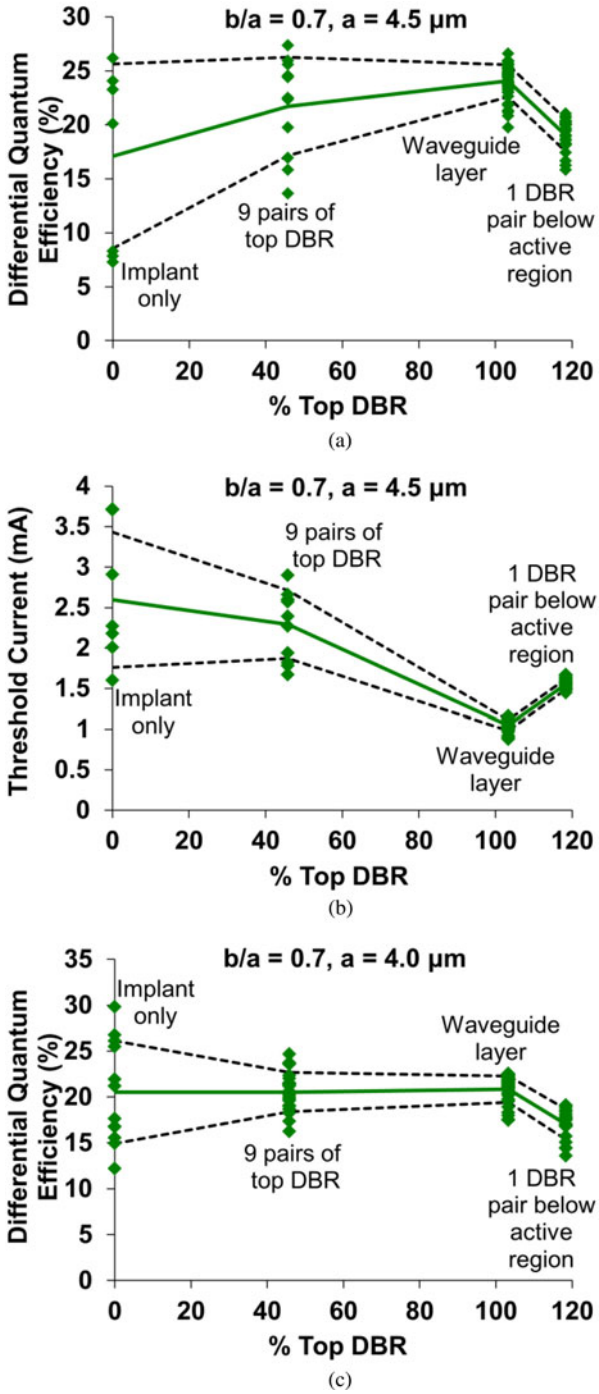

Fig. 3. (a) Differential quantum efficiency and (b) threshold current versus etch depth (normalized to top DBR mirror thickness) for photonic crystal VCSELs with $b/a = 0.7$, $a = 4.5$ um. (c) Differential quantum efficiency versus etch depth for photonic crystal VCSELs with $b/a = 0.7$, $a = 4.0$ um. The data points at each etch depth correspond to different devices with the same design from Sample A. The solid line indicates the average, whereas the dashed lines coincide with the standard deviation of the measurements.

where n_{core} is the effective index of the core, n_{clad} is the effective index of the cladding obtained from the effective index method, $n_{\text{core,holes}}$ is the effective cladding index assuming infinite etch depth, and Δn_{eff} is the index contrast assuming infinite etch depth.

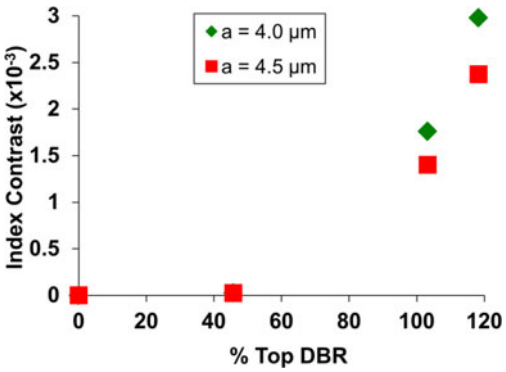

Fig. 4. Index contrast (Δn) as a function of etch depth. Diamonds represent $a = 4.0$ μm and squares represent $a = 4.5$ μm. For $a = 4.5$ μm, Δn increases slower with respect to etch depth and Δn is in general lower than photonic crystal VCSELs with $a = 4.0$ μm for the same etch depth.

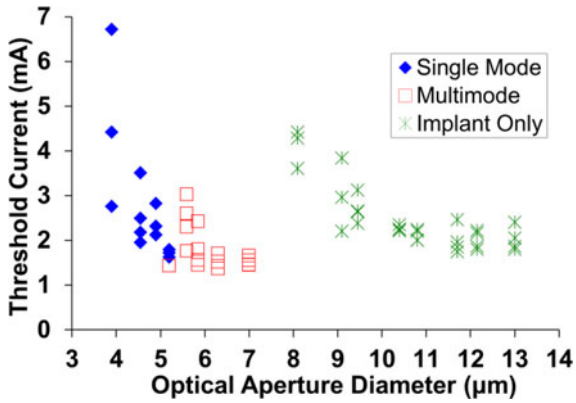

Fig. 5. Threshold current as a function of optical aperture diameter.

Referring to Fig. 3(a), for $a = 4.5$ μm, the differential quantum efficiency gradually increases with etch depth until reaching the active region, because of reduced diffraction, scattering, and mirror loss arising from the increased index contrast with increased etch depth. From Fig. 4, we see that for a pitch of $a = 4.5$ μm, the index contrast increases slower with respect to etch depth and Δn is lower than for photonic crystal VCSELs with $a = 4.0$ μm for the same etch depth. As a result, the transverse modes of photonic crystal VCSELs with $a = 4.5$ μm have greater spatial overlap with the photonic crystal cladding; hence, these photonic crystal VCSELs are more susceptible to optical loss introduced by the photonic crystal cladding especially for shallow etch depths. For a pitch of $a = 4.0$ μm shown in Fig. 3(c), the increase of differential quantum efficiency with etch depth is not as obvious, at least partially due to more tightly confined transverse mode profile. For all photonic crystal designs, the differential quantum efficiency decreases when the holes perforate the quantum-well active region, presumably due to nonradiative recombination [35] creating increased heating and carrier leakage [36].

The threshold current of the photonic crystal VCSELs monotonically decreases with deeper etch depth as evident in Fig. 3(b), due to the reduced optical loss from the increased index contrast. However, when the air holes are etched through the active region, the photonic crystal VCSELs have increased threshold current due to nonradiative recombination. From the results of Figs. 3 and 4, we conclude that etching the photonic crystal through the top DBR to the top of the active region yields the best VCSEL performance in terms of high differential quantum efficiency and low threshold current. Note that defining a smaller proton-implanted gain aperture than the optical cavity could prevent carrier diffusion to the exposed quantum well edges, but at the expense of increasing the current density.

The performance of photonic crystal VCSELs with hole etch depth is similar to that found for etched air-post VCSELs [35]. A shallow etch depth results in diffraction, whereas etching through the active region creates nonradiative recombination. The transverse index profile can be designed by the etch depth for both photonic crystal and air-post VCSELs, but the higher resulting index step of the air-post VCSEL demands smaller device diameter to enable single-mode operation [37].

In Fig. 5, the threshold current versus the optical aperture diameter of VCSELs fabricated from Sample A is shown. The photonic crystal VCSELs in this plot employ the optimum design of etching the holes through the top DBR. The optical aperture diameter is taken from the photonic crystal design; for the proton-implanted VCSELs, we use the implant diameter. For the photonic crystal VCSELs, we indicate in Fig. 5 which VCSELs operate single fundamental mode, and which exhibit multimode operation. Threshold current in general decreases after the photonic crystal is introduced except for devices with the smallest implant apertures (compare single-mode photonic crystal VCSELs with aperture of 3.9 μm and implanted VCSELs with aperture of 8.1 μm). The VCSELs with the smallest implant aperture experience greater heating than larger diameter VCSELs, and hence, the index confinement arising from the photonic crystal has minimal effect on reducing diffraction loss and threshold current. A photonic crystal optical aperture of 5.2 μm and less tends to yield single-mode lasing, even for the condition of blue-shifted gain peak. In general, output power scales with optical aperture diameter, so larger aperture (~ 5 μm) is preferred if higher single-mode optical power is desired.

IV. Conclusion

Planar index-guided proton-implanted photonic crystal VCSELs are fabricated and characterized. We use photonic crystal designs that are accessible to standard fabrication processes and lead to fundamental mode operation with $\geq$30-dB SMSR from threshold to maximum power. The photonic crystal VCSELs are thus shown to be manufacturable due to their planar topology, the use of optical lithography in all processing steps, and compatibility with virtually any VCSEL epitaxial designs. They are also superior in performance compared to gain-guided VCSELs due to their stable output characteristics, increased differential quantum efficiency, reduced threshold current, and single-mode operation even for the condition of blue-shifted gain peak relative to the cavity resonance. With proper photonic crystal and aperture size design, single-mode output power of $>$2.5 mW can be obtained. Photonic crystal VCSELs with less blue-shifted gain would be expected to have lower threshold

current, higher output power, and operate in single mode even with larger optical aperture for reduced beam divergence. Finally, the increased gain diameter provided by the proton implantation leads to low current density operation, from which excellent reliability can be expected.

ACKNOWLEDGMENT

The authors would like to thank Finisar Corporation for providing epitaxial VCSEL material used in this study.

REFERENCES

[1] K. D. Choquette and K. M. Geib, "Fabrication and performance of vertical-cavity surface-emitting lasers," in *Vertical-Cavity Surface-Emitting Lasers*, C. Wilmsen, H. Temkin, and L. A. Coldren, Eds. New York, NY, USA: Cambridge Univ. Press UP, 1999, pp. 193–232.

[2] K. D. Choquette, R. P. SchneiderJr., K. L. Lear, and K. M. Geib, "Low threshold voltage vertical-cavity lasers fabricated by selective oxidation," *Electron. Lett.*, vol. 30, no. 24, pp. 2043–2044, Nov. 1994.

[3] Y. H. Lee, B. Tell, K. Brown-Goebeler, J. L. Jewell, and J. V. Hove, "Top-surface emitting GaAs four-quantum-well lasers emitting at 0.85 μm," *Electron. Lett.*, vol. 26, no. 11, pp. 710–711, May 1990.

[4] N. K. Dutta, L. W. Tu, G. Zydzik, G. Hasnain, Y. H. Wang, and A. Y. Cho, "Anomalous temporal response of gain guided surface emitting lasers," *Electron. Lett.*, vol. 27, no. 3, pp. 208–210, Jan. 1991.

[5] K. L. Lear, R. P. SchneiderJr., K. D. Choquette, and S. P. Kilcoyne, "Index guiding dependent effects in implant and oxide confined vertical-cavity lasers," *IEEE Photon. Technol. Lett.*, vol. 8, no. 6, pp. 740–742, Jun. 1996.

[6] K. D. Choquette, K. M. Geib, Ro. D. Briggs, A. A. Allerman, and J. J. Hindi, "Single transverse mode selectively oxidized vertical cavity lasers," *Proc. SPIE*, vol. 3946, pp. 230–233, 2000.

[7] E. W. Young, K. D. Choquette, S. L. Chuang, K. M. Geib, A. J. Fischer, and A. A. Allerman, "Single-transverse-mode vertical-cavity lasers under continuous and pulsed operation," *IEEE Photon. Technol. Lett.*, vol. 13, no. 9, pp. 927–929, Sep. 2001.

[8] H. J. Unold, S. W. Z. Mahmoud, R. Jäger, M. Kicherer, M. C. Riedl, and K. J. Ebeling, "Improving single-mode VCSEL performance by introducing a long monolithic cavity," *IEEE Photon. Technol. Lett.*, vol. 12, no. 8, pp. 939–941, Aug. 2000.

[9] N. Nishiyama, M. Arai, S. Shinada, K. Suzuki, F. Koyama, and K. Iga, "Multi-oxide layer structure for single-mode operation in vertical-cavity surface-emitting lasers," *IEEE Photon. Technol. Lett.*, vol. 12, no. 6, pp. 606–608, Jun. 2000.

[10] P. D. Floyd, M. G. Peters, L. A. Coldren, and J. L. Merz, "Suppression of higher-order transverse modes in vertical-cavity lasers by impurity-induced disordering," *IEEE Photon. Technol. Lett.*, vol. 7, no. 12, pp. 1388–1390, Dec. 1995.

[11] J.-W. Shi, C.-C. Chen, Y.-S. Wu, S.-H. Guol, C. Kuo, and Y.-J. Yang, "High-power and high-speed Zn-diffusion single fundamental-mode vertical-cavity surface-emitting lasers at 850-nm wavelength," *IEEE Photon. Technol. Lett.*, vol. 13, no. 13, pp. 1121–1123, Jul. 2008.

[12] Y. A. Wu, G. S. Li, R. F. Nabiev, K. D. Choquette, C. Caneau, and C. J. C. Hasnain, "Single-mode, passive antiguide vertical cavity surface emitting laser," *IEEE J. Sel. Topics Quantum Electron.*, vol. 1, no. 2, pp. 629–637, Jun. 1995.

[13] D. Zhou and L. Mawst, "High-power single-mode antiresonant reflecting optical waveguide-type vertical-cavity surface-emitting lasers," *IEEE J. Quantum Electron.*, vol. 38, no. 12, pp. 1599–1606, Dec. 2002.

[14] R. A. Morgan, G. D. Guth, M. W. Focht, M. T. Asom, K. Kojima, L. E. Rogers, and S. E. Callis, "Transverse mode control of vertical-cavity top-surface-emitting lasers," *IEEE Photon. Technol. Lett.*, vol. 4, no. 4, pp. 374–377, Apr. 1993.

[15] P. Dowd, L. Raddatz, Y. Sumaila, M. Asghari, I. H. White, R. V. Penty, P. J. Heard, G. C. Allen, R. P. Schneider, M. R. T. Tan, and S. Y. Wang, "Mode control in vertical-cavity surface-emitting lasers by post-processing using focused ion-beam etching," *IEEE Photon. Technol. Lett.*, vol. 9, no. 9, pp. 1193–1195, Sep. 1997.

[16] H. Martinsson, J. A. Vukušić, M. Grabherr, R. Michalzik, R. Jäger, K. J. Ebeling, and A. Larsson, "Transverse mode selection in large-Area oxide-confined vertical-cavity surface-emitting lasers using a shallow surface relief," *IEEE Photon. Technol. Lett.*, vol. 11, no. 12, pp. 1536–1538, Dec. 1999.

[17] A. C. Lehman, E. A. Yamaoka, C. W. Willis, K. D. Choquette, K. M. Geib, and A. A. Allerman, "Variable reflectance vertical cavity surface emitting lasers," *Electron. Lett.*, vol. 43, no. 8, pp. 460–461, Apr. 2007.

[18] J. E. Cunningham, D. K. McElfresh, L. D. Lopez, D. Vacar, and A. V. Krishnamoorthy, "Scaling vertical-cavity surface emitting laser reliability for petascale systems," *Appl. Opt.*, vol. 45, no. 25, pp. 6342–6348, Sep. 2006.

[19] H. J. Unold, M. Golling, R. Michalzik, D. Supper, and K. J. Ebeling, "Photonic crystal surface-emitting lasers: Tailoring waveguide for single-mode emission," in *Proc. 27th Eur. Conf. Optical Commun.*, Amsterdam, The Netherlands, 2001, pp. 520–521.

[20] D. S. Song, S. H. Kim, H. G. Park, C. K. Kim, and Y. H. Lee, "Single-fundamental-mode photonic-crystal vertical-cavity surface-emitting lasers," *Appl. Phys. Lett.*, vol. 80, no. 21, pp. 3901–3903, May 2002.

[21] N. Yokouchi, A. J. Danner, and K. D. Choquette, "Two-dimensional photonic crystal confined vertical-cavity surface-emitting lasers," *IEEE J. Sel. Topics Quantum Electron.*, vol. 9, no. 5, pp. 1439–1445, Sep./Oct. 2003.

[22] J.-H. Baek, D.-S. Song, I.-K. Hwang, K.-H. Lee, and Y. H. Lee, "Transverse mode control by etch-depth tuning in 1120-nm GaInAs/GaAs photonic crystal vertical-cavity surface-emitting lasers," *Opt. Exp.*, vol. 12, no. 5, pp. 859–867, Mar. 2004.

[23] H. P. D. Yang, F. I. Lai, Y. H. Chang, H. C. Yu, C. P. Sung, H. C. Kuo, S. C. Wang, S. Y. Lin, and J. Y. Chi, "Singlemode (SMSR $>$ 40 dB) proton implanted photonic crystal vertical-cavity surface-emitting lasers," *Electron. Lett.*, vol. 41, no. 6, pp. 326–328, Mar. 2005.

[24] P. O. Leisher, J. D. Sulkin, and K. D. Choquette, "Parametric study of proton-implanted photonic crystal vertical-cavity surface-emitting lasers," *IEEE J. Sel. Topics Quantum Electron.*, vol. 13, no. 5, pp. 1290–1294, Sep.–Oct. 2007.

[25] A. M. Kasten, M. P. Tan, J. D Sulkin, P. O. Leisher, and K. D. Choquette, "Photonic crystal vertical cavity lasers with wavelength-independent single-mode behavior," *IEEE Photon. Technol. Lett.*, vol. 20, no. 23, pp. 2010–2012, Dec. 2008.

[26] A. M. Kasten, J. D. Sulkin, P. O. Leisher, D. K. Mc Elfresh, D. Vacar, and K. D. Choquette, "Manufacturable photonic crystal single mode and fluidic vertical cavity surface emitting lasers," *IEEE J. Sel. Topics Quantum Electron.*, vol. 14, no. 4, pp. 1123–1131, Jul./Aug. 2008.

[27] D. F. Siriani, P. O. Leisher, and K. D. Choquette, "Loss-induced confinement in photonic crystal vertical-cavity surface-emitting lasers," *IEEE J. Quantum Electron.*, vol. 45, no. 7, pp. 762–768, Jul. 2009.

[28] D. B. Young, J. W. Scott, F. H. Peters, M. G. Peters, M. L. Majewski, B. J. Thibeault, S. W. Corzine, and L. A. Coldren, "Enhanced performance of offset-gain high-barrier vertical-cavity surface-emitting lasers," *IEEE J. Quantum Electron.*, vol. 29, no. 6, pp. 2013–2022, Jun. 1993.

[29] Y. Kaneko, T. Tamanuki, M. Katoh, H. Maekawa, F. Koyama, and K. Iga, "Transverse-mode characteristics of InGaA/GaAs vertical-cavity surface-emitting lasers considering gain offset," *Jpn. J. Appl. Phys.*, vol. 32, no. 11A, pp. L1612–L1614, Nov. 1993.

[30] J. K. Guenter, J. A. Tatum, A. Clark, R. S. Penner, R. H. Johnson, R. A. Hawthorne, J. R. Biard, and Y. Liu, "Commercialization of Honeywell's VCSEL technology: Further developments," *Proc. SPIE*, vol. 4286, pp. 1–14, 2001.

[31] D. Vakhshoori, J. D. Wynn, G. J. Zydzik, R. E. Leibenguth, M. T. Asom, K. Kojima, and R. A. Morgan, "Top-surface emitting lasers with 1.9 V threshold voltage and the effect of spatial hole burning on their transverse mode operation and efficiencies," *Appl. Phys. Lett.*, vol. 62, no. 13, pp. 1448–1450, Mar. 1993.

[32] A. J. Danner, T. S. Kim, and K. D. Choquette, "Single fundamental mode photonic crystal vertical cavity laser with improved output power," *Electron. Lett.*, vol. 41, no. 6, pp. 325–326, Mar. 2005.

[33] K. D. Choquette, K. L. Lear, R. P. SchneiderJr., and K. M. Geib, "Cavity characteristics of selectively oxidized vertical-cavity lasers," *Appl. Phys. Lett.*, vol. 66, no. 25, pp. 3413–3415, Jun. 1995.

[34] G. R. Hadley, "Effective index model for vertical-cavity surface-emitting lasers," *Opt. Lett.*, vol. 20, no. 13, pp. 1483–1485, Jul. 1995.

[35] K. D. Choquette, G. Hasnain, Y. Wang, J. Wynn, R. S. Freund, and A. Y. Cho, "GaAs vertical-cavity surface emitting lasers fabricated by reactive ion etching," *IEEE Photon. Technol. Lett.*, vol. 3, no. 10, pp. 859–862, Oct. 1991.

[36] J. W. Scott, R. S. Geels, S. W. Corzine, and L. A. Coldren, "Modeling temperature effects and spatial hole burning to optimize vertical-cavity surface-emitting laser performance," *IEEE J. Quantum Electron.*, vol. 29, no. 5, pp. 1295–1308, May 1993.

[37] C. J. Chang-Hasnain, M. Orenstein, A. Von Lehmen, L. T. Florez, J. P. Harbison, and N. G. Stoffel, "Transverse mode characteristics of vertical cavity surface-emitting lasers," *Appl. Phys. Lett.*, vol. 57, no. 3, pp. 218–220, Jul. 1990.

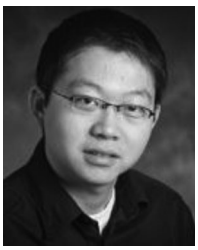

Meng Peun Tan (S'08) received the B.S. and M.S. degrees in electrical engineering from the University of Illinois at Urbana-Champaign, Urbana, IL, USA, in 2007 and 2009, respectively, where he is currently working toward the Ph.D. degree in electrical engineering.

His current research interests include mode control in semiconductor lasers, various high-speed modulation approaches in vertical-cavity surface-emitting lasers, and passive devices in optical interconnects.

Mr. Tan is a student member of the IEEE photonics Society (formerly the Lasers and Electro-Optics Society).

Ansas M. Kasten received the Dipl.Ing. degree in electrical engineering from the University of Saarland, Saarbrucken, Germany, in 2003, and the M.S. and the Ph.D. degrees in electrical engineering from the University of Illinois at Urbana-Champaign, Urbana, IL, USA, in 2006 and 2010, respectively.

He is currently a member of the Photonics Laboratory, General Electric Global Research Center, Niskayuna, NY, USA. His current research interests include vertical-cavity surface-emitting lasers (VCSELs), VCSEL arrays, and detector arrays for communication and biosensing applications.

Joshua D. Sulkin received the B.S., M.S., and Ph.D. degrees in electrical and computer engineering from the University of Illinois at Urbana-Champaign, Urbana, IL, USA, in 2006, 2007, and 2012, respectively.

As a graduate student in the Photonics Device Research Group, he studied optoelectronics and computational electromagnetics. He is currently a Flight Software Engineer at Space Exploration Technologies Corporation, Hawthorne, CA, USA, developing software and algorithms for the Falcon launch vehicle and Dragon spacecraft.

Kent D. Choquette (M'97–F'03) received the B.S. degrees in engineering physics and applied mathematics from the University of Colorado-Boulder, Boulder, CO, USA, and the M.S. and Ph.D. degrees in materials science from the University of Wisconsin-Madison, Madison, WI, USA.

He was a Postdoctoral Researcher at AT&T Bell Laboratories, Murray Hill, NJ, USA, and then joined Sandia National Laboratories, Albuquerque, NM, USA. In 2000, he joined the Department of Electrical and Computer Engineering, University of Illinois at Urbana-Champaign, Urbana, IL, USA, and was named the Able Bliss Professor of Engineering. His Photonic Device Research Group is centered around the design, fabrication, characterization, and applications of vertical-cavity surface-emitting lasers, photonic crystal light sources, nanofabrication technologies, and hybrid integration techniques. He has authored more than 200 technical publications and five book chapters, and has presented numerous invited talks and tutorials.

Dr. Choquette is a Fellow of the Optical Society of America (OSA), a Fellow of the International Society for Optics and Photonics, and a Fellow of the American Association for the Advancement of Science. He was awarded the 2012 OSA Nick Holonyak Jr. Award and the 2008 IEEE/ Lasers and Electro-Optics Society (LEOS) Engineering Achievement Award. From 2000 to 2002, he was an IEEE/LEOS Distinguished Lecturer. He has served as an Associate Editor of the IEEE JOURNAL OF QUANTUM ELECTRONICS, the IEEE PHOTONIC TECHNOLOGY LETTERS, and the JOURNAL OF LIGHTWAVE TECHNOLOGY, as well as a Guest Editor of the IEEE JOURNAL OF SELECTED TOPICS IN QUANTUM ELECTRONICS.